Chinese Chemical Letters 35 (2024) 109754

Contents lists available at ScienceDirect

Chinese Chemical Letters

journal homepage: www.elsevier.com/locate/cclet

Microfluidic-based isolation of circulating tumor cells with high-efficiency and high-purity

Feng Wu[b,1], Xuemin Kong[a,1], Yixuan Liu[b], Shuli Wang[a,*], Zhong Chen[a,e,*], Xu Hou[c,d,e]

[a] Fujian Engineering Research Center for Solid-State Lighting, Department of Electronic Science, School of Electronic Science and Engineering, Xiamen University, Xiamen 361005, China
[b] College of Physics and New Energy, Xuzhou University of Technology, Xuzhou 221018, China
[c] State Key Laboratory of Physical Chemistry of Solid Surfaces, College of Chemistry and Chemical Engineering, Xiamen University, Xiamen 361005, China
[d] College of Physical Science and Technology, Xiamen University, Xiamen 361005, China
[e] Innovation Laboratory for Sciences and Technologies of Energy Materials of Fujian Province (IKKEM), Xiamen 361102, China

ARTICLE INFO

Article history:
Received 10 January 2024
Revised 29 February 2024
Accepted 5 March 2024
Available online 11 March 2024

Keywords:
Microfluidics
Isolation
Circulating tumor cells
High-efficiency
High-purity

ABSTRACT

The isolation of circulating tumor cells (CTCs) from complex biological samples is of paramount significance for advancing cancer diagnosis, prognosis, and treatment. However, the low concentration of CTCs and nonspecific adhesion of white blood cells (WBCs) present challenges that hinder the efficiency and purity of captured CTCs. Microfluidic-based strategies utilize precise fluid control at the micron level to incorporate specific micro/nanostructures or recognition molecules, enabling effective CTCs separation. Moreover, by employing surface modification designs that exhibit exceptional anti-adhesion properties against WBCs, the purity of isolated CTCs can be further enhanced. This review offers an in-depth exploration of recent advancements, challenges, and opportunities associated with microfluidic-based CTCs isolation from biological samples. Firstly, we will comprehensively introduce the microfluidic-based strategies for achieving high-efficiency CTCs isolation, which includes the morphological design of microchannels for physical force-based CTCs isolation and the specific modification of microchannel surfaces for affinity-based CTCs isolation. Subsequently, a review of recent research advances in microfluidic-based high-purity CTCs isolation is presented, focusing on strategies that decrease the nonspecific adhesion of WBCs through surface micro-/nanostructure construction or chemical and biological modification. Finally, we will summarize the article by providing the prospective opportunities and challenges for the future development of microfluidic-based CTCs isolation.

1. Introduction

Malignant neoplasm, commonly known as a cancerous tumor, is a significant contributor to global fatalities. Predictions indicate that the worldwide incidence of new cancer cases is projected to reach 20.3 million by 2030, with approximately 13.2 million cancer-related deaths, highlighting the urgent need to address this crucial public health issue [1,2]. The fatal outcomes of malignant tumors predominantly stem from uncontrolled growth, invasion of surrounding tissues, metastasis, and the disruption of vital organ function [3]. Among these factors, tumor metastasis plays a particularly critical role, accounting for a staggering 90% of mortality related to cancer [4–6]. Early detection and ongoing research are essential in the development of effective strategies to combat cancer and reduce mortality associated with malignant tumors [7,8].

CTCs detection plays a crucial role in early cancer screening as it enables the identification of cancer in its earliest and most treatable stages [9–11]. CTCs are cancer cells that have detached from the primary tumor and entered the bloodstream. These cells possess the ability to migrate to different parts of the body and initiate the formation of new tumors, a process known as metastasis. Clinical studies have demonstrated that an inverse relationship between the quantity of CTCs present and patient survival rates [12]. Additionally, reducing or eliminating CTCs following initial or adjuvant therapy has been shown to prolong survival [13]. Therefore, the isolation of CTCs can provide valuable insights into tumor metastasis, the response of cancer to therapeutic interventions, and facilitate personalized treatment plans for individuals with tumors.

The isolation of CTCs from blood samples poses significant challenges due to several reasons. Firstly, the low concentration of CTCs

* Corresponding authors.
E-mail addresses: slwang@xmu.edu.cn (S. Wang), chenz@xmu.edu.cn (Z. Chen).
[1] These authors contributed equally to this work.

https://doi.org/10.1016/j.cclet.2024.109754
1001-8417/

(a few to hundreds per milliliter) compared to red blood cells (RBCs) (10^9–10^{10} per milliliter) and WBCs (10^6–10^7 per milliliter) in the blood requires sensitive and specific methods to differentiate them from other blood cells and contaminants [14,15]. This is crucial for accurate identification and analysis of CTCs. Secondly, the inherent heterogeneity of CTCs, characterized by significant variations in physical properties and biological properties, further increases the challenge of CTCs separation. Thirdly, non-specific adhesion of WBCs to the isolation platform or CTCs capture agents leads to the contamination and false-positive results, compromising the accuracy and reliability of downstream analyses [16,17]. Hence, it is essential to develop the innovative technologies and approaches that can overcome these obstacles and enable high-efficiency and high-purity isolation of CTCs.

Until now, several approaches including filtration [18], density gradient centrifugation [19], micro/nanostructured surface [20,21], immunoaffinity [22], and microfluidic-based strategies [23] have been proposed for the isolation of CTCs based on differences in their physical properties (such as size [24], deformability [25], electric charges [26]) and biological properties (such as cell surface protein expression [27]) compared to normal blood cells. Among these approaches, microfluidic-based strategies offer significant advantages in isolation of CTCs due to their low sample consumption, rapid and continuous processing, gentle and efficient cell handling, low cost, *etc*. [28–30]. Microfluidic technology enables precise manipulation of blood cells in biological fluids, which enables the separation of CTCs from other blood components based on their distinct physical properties [31,32]. Furthermore, specific surface modifications can be applied to the microchannel surfaces, utilizing the unique expressed proteins of CTCs to selectively capture target CTCs from the complex mixture of components [33]. Additionally, the micro-/nanostructures construction or bio/chemical modifications on the microchannel surfaces can reduce the nonspecific adhesion of WBCs to increase the purity of the isolated CTCs [34–38]. Therefore, microfluidic technology is a highly promising technology for achieving high-efficient and high-purity capture of CTCs, which is of great significance for subsequent clinical detection such as protein profiling, genetic characterization, heterogeneity analysis, and drug sensitivity testing.

In this review, we provide a comprehensive overview of the emerging microfluidic-based strategies for the high-efficiency and high-purity isolation of CTCs (Fig. 1). Firstly, we will introduce the microfluidic-based strategies for achieving high-efficiency CTCs isolation, including physical force-based and affinity-based strategies. Subsequently, we review the microfluidic chip with surface modification strategies that enable high-purity CTCs isolation, including surface topographical micro-/nanostructures design, surface chemical modification strategies, and surface biological modification strategies. Finally, we conclude the article by discussing the challenges associated with achieving high-efficiency and high-purity CTCs isolation, as well as the future developments in this rapidly advancing research field.

2. High-efficiency isolation of CTCs

2.1. Physical force-based strategies

Physical force-based strategies utilize the differences in physical characteristics of CTCs and normal blood cells, such as size [39,40], deformability [41], and electrical properties [42] to isolate CTCs from biological samples. In this section, we will discuss some representative physical force-based microfluidic strategies including size-based CTCs separation, hydrodynamics-based CTCs separation, and dielectrophoresis (DEP)-based CTCs separation, which is established based on the above inherent characteristics to overcome the challenges of low CTCs concentrations and achieve efficient isolation of CTCs from biological samples.

2.1.1. Size-based CTCs separation

Size-based CTCs separation relies on the porous filters with specific pore size to isolate the CTCs from the biological fluid through selectively allowing the passage of blood cells while retaining CTCs [24]. CTCs typically exhibit larger diameters, ranging from 14 μm to 26 μm, compared to the smaller diameters of WBCs which range from 8 μm to 20 μm. When the blood sample flows through the chip containing filter structures of specific size, the larger CTCs are unable to pass through the filter based on the size effect, while normal blood cells can flow through the filters and are carried away with the buffer flow, leading to the isolation of CTCs.

Hosokawa *et al.* fabricated a microfluidic chip with nickel-based microcavity array filter for isolating the CTCs from blood sample [43]. Using electroforming technology, they created a 100×100 nickel-based circular microcavity filter with a diameter range of 8 μm to 9 μm. As the cells and buffer flowed through these circular pores, the larger-sized CTCs were effectively captured on the microfilters. Their experimental results show that the microfluidic system was capable of processing 1 mL of blood containing 10 spiked tumor cells within 15 min, and the separation efficiency reached 97%.

Separating CTCs from blood samples with a high concentration of blood cells often leads to clogging in microfilters, which in turn reduces the efficiency of CTCs separation and compromises the viability of the CTCs. To overcome the issue, Chen *et al.* developed a microfluidic chip incorporating a lateral filter array with embedded filters in a serpentine main channel to effectively minimize filter clogging and reduce potential damage to CTCs [44]. The microfluidic chip demonstrated the highest capture efficiency of 82.3% for MCF-7 cells at a flow rate of 1.8 mL/h. Additionally, the viability of released L3.6pl cells from this chip was 92.9%, a value comparable to the pre-infusion cell viability of 96.1%.

The development of the CTCs capture strategy that enables simultaneous identification of cancer subpopulation response is also crucial in providing additional information for patients' prognosis and treatment. Zhang *et al.* introduced a microfluidic chip with asymmetric T-shaped pillar structures for the *in-situ* isolation and profiling of CTCs [45]. These structures were designed with varying gap sizes of 8, 10, 12, 14, and 16 μm, featuring protrusions or extended regions. The specific structures provide extra contact points for cell adhesion, thereby increasing the available surface area for the isolation of the CTCs. As samples containing CTCs passed through the microfluidic device, the two T-shaped pillar structures effectively captured larger CTCs while simultaneously filtering out contaminating blood cells. Their results showed that the capture efficiency varies with the size of the gap, and the highest capture efficiency of 93% ± 6% for MCF-7 cells was achieved when the size of the gap was 12 μm. In addition, the utilization of aptamer nanovectors, composed of a spherical gold nanoparticle core and a thin silver shell with strong surface-enhanced Raman (SERS) properties, allows for *in-situ* cancer subpopulation detection through spectral SERS signal analysis. This comprehensive approach not only facilitates CTCs isolation but also enables their characterization based on specific cancer-related markers.

In addition to the single CTCs, CTCs clusters are even rarer in circulation but are more valuable in terms of predicting transitions than the single CTCs. As CTCs clusters consist of more than two tumor cells and possess larger diameters than blood cells, the latter can easily navigate through the chip containing filter structures. In contrast, CTCs clusters, being too large to pass through individual openings, commit to constrictions and are effectively captured [46]. Sarioglu *et al.* introduced the Cluster-Wells chip, featuring a micromesh with openings of 15 μm × 15 μm at the bottom of each

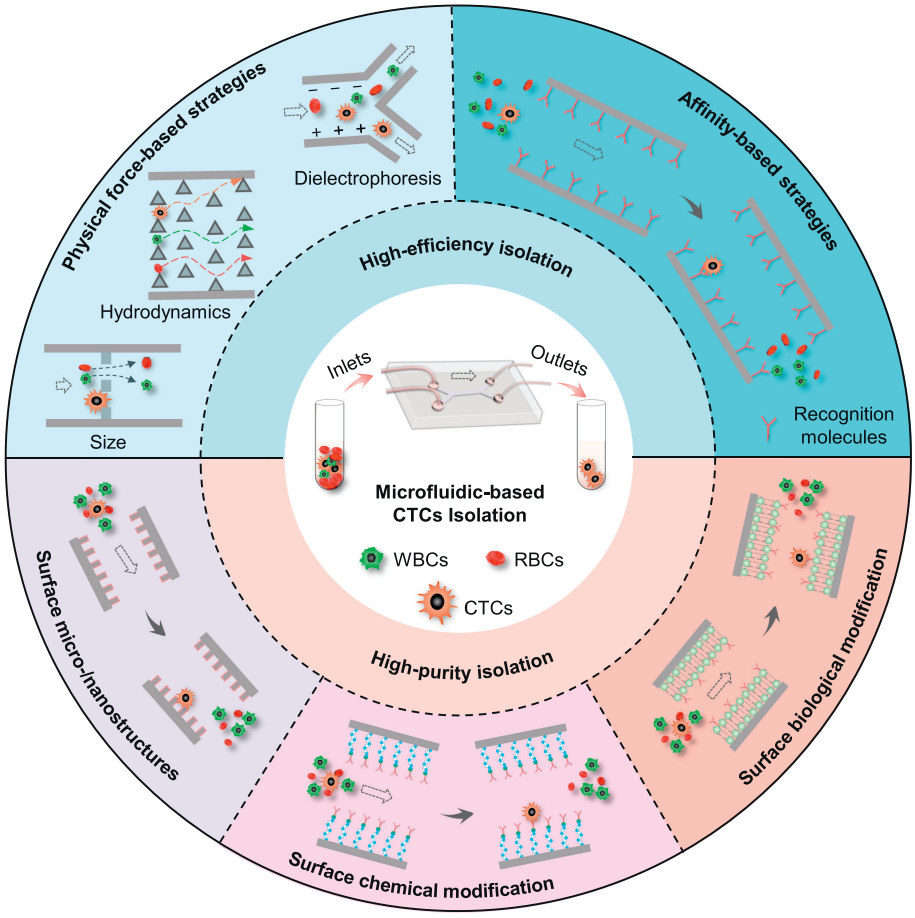

Fig. 1. Schematic illustration of microfluidic-based strategies for high-efficiency and high-purity isolation of CTCs.

well (Fig. 2A) [47]. This specific size allows leukocytes, erythrocytes, and platelets to pass unimpeded, while larger CTC clusters get captured within the cluster lodge in neighboring mesh openings. Once CTC clusters enter the microwells, they become confined within the grid due to the slanted sidewalls, while 2 μm-wide mesh lines ensure the entry of cell clusters into different openings. Their findings indicated that a capture efficiency of 96% for LNCaP clusters and 87% for MDA-MB-231 clusters was achieved at a flow velocity of 6.5 mm/s.

2.1.2. Hydrodynamics-based CTCs separation

Hydrodynamics-based separation strategies use the different flow behavior exhibited by CTCs and normal blood cells under fluid dynamics to isolate CTCs from the biological fluid [48,49]. By injecting the biological fluid into a microchannel containing microstructure arrays, CTCs, WBCs, and RBCs show distinct flow pathways under the shear gradient lift force and wall-effect lift force, which enables the different types of suspended cells can be collected from the different outlets [50].

Park *et al.* developed a microfluidic platform consisting of a conical contraction matrix with 32 rows and 2048 columns to achieve efficient separation of CTCs [25]. When the whole blood sample is injected from the lower left corner into the conical contraction matrix, cells are driven by two flow forces: one from the oscillating inlet with the biased oscillating flow and the other from the buffer inlet with a steady right flow. The spacing between rows remains uniform, whereas the distance between columns progressively increases along the vertical dimension of the matrix, ranging from 1 μm to 18 μm. Smaller RBCs and easily deformable WBCs traverse through the narrow funnel, while the CTCs effectively restricted between two adjacent rows and subsequently collected through a continuous rightward flow. The implementation of this microfluidic chip yielded a notably consistent CTCs separation efficiency ranging from 93% to 96%.

Deterministic lateral displacement (DLD) microfluidic chips utilize the micropost arrays with a certain angled relative to the fluid flow direction within the chip to induce different flow trajectories for CTCs and normal blood cells to isolate CTCs. When the biological fluid is injected a DLD chip, larger CTCs experience controlled lateral displacement, while smaller blood cells follow their original trajectories, enabling the effective isolation of CTCs. Until now, researchers have designed various DLD chips with different microstructures to separate the CTCs from the blood samples [51,52]. Au *et al.* introduced a two-stage DLD separation array that combined asymmetric I-shaped pillars and elliptic cylinders and achieved a capture efficiency of 99% for CTCs clusters cultured from patients with breast cancer [53]. The asymmetric pillars with a height of 30 μm and spaced 63 μm apart, along with row shift ratios of 1/7, were designed to isolate CTCs from the blood sample without clogging. In addition, the CTCs encountered lower shear stress rates in the microchannel, which effectively minimized the damage for the captured CTCs with viability exceeding 87%. These findings suggest that DLD microfluidic chips offer a promising approach for efficient and gentle isolation of CTCs for further analysis and characterization.

Liu *et al.* employed a microfluidic DLD chip that comprises two modules, in which the first module comprised two mirrored DLD microarrays for negative selection of CTCs and the second module with a DLD array with an increasing tilting angle to separate the CTCs [54]. The triangular microposts were 30 μm on each

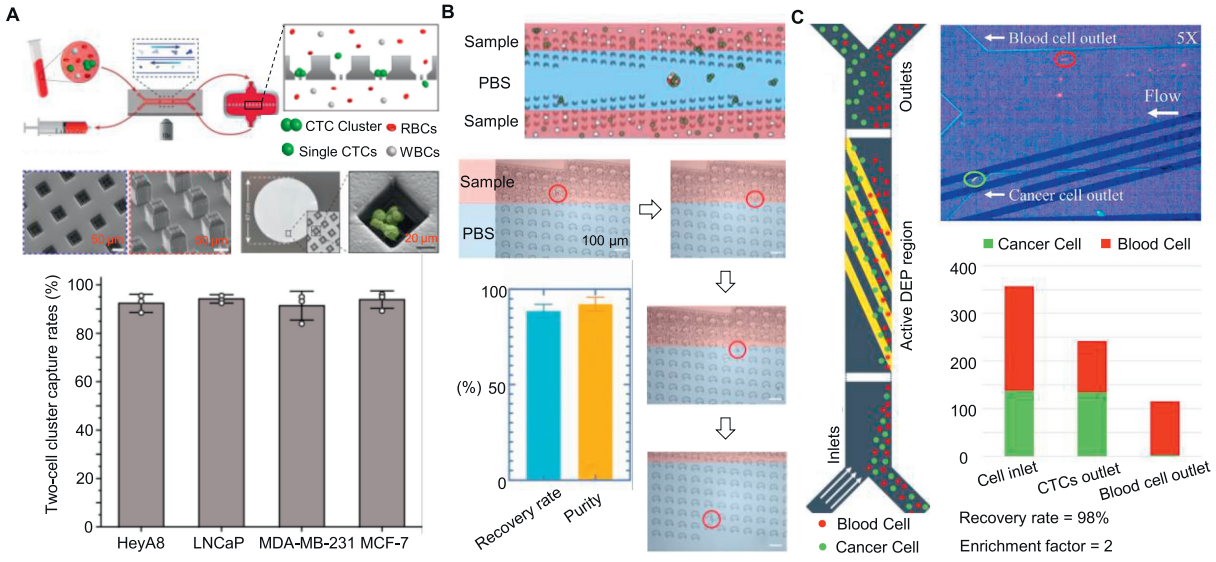

Fig. 2. Physical force-based high-efficiency isolation of CTCs in microfluidic chips. (A) Schematic illustration of the working mechanism of Cluster-Wells chip for the isolation of CTCs clusters. SEM images of the well structure, a blood-spiked LNCaP cluster captured within a well, and the dual-cell cluster capture efficiency for LNCaP, MDA-MB-231, MCF-7, and HeyA8 cancer cells. Reproduced with permission [47]. Copyright 2022, Springer Nature. (B) Schematic of the DLD cluster sorting module for the separation of CTCs clusters. The red circles highlight the trajectories of CTCs 4T1 cancer cells within the DLD microarrays. The recovery rate and purity of capture of 4T1 clusters. Reproduced with permission [55]. Copyright 2023, Elsevier. (C) The schematic illustration of a microchannel with electrodes for isolation of CTCs based on DEP. The microscopy images show the WBCs (red) and MCF-7 cells (green) progressing toward the different outlets under electric force. The number of the CTCs and blood cells entered from the inlet and exited from the outlets. Reproduced with permission [60]. Copyright 2022, Wiley-VCH.

side, 30 μm in height, and 25 μm in gap between the neighboring posts. In the first module, the RBCs moved along the fluid direction, while CTCs and WBCs moved at the angle of the micropost arrays, leading to the isolation of the CTCs and WBCs from the RBCs. In the second module, the target CTCs moved along the tilted array, while the majority of WBCs moved in the direction of the fluid, resulting in the separation of CTCs and the WBCs. The experimental results showed the integrated microfluidic DLD chip achieved a capture efficiency exceeding 90% for both the MDA-MB-231 and the MCF-7 cells as the flow rate increased from 6 mL/h to 18 mL/h.

The critical diameter is pivotal for differentiating cells based on size in DLD. However, the presence of CTCs clusters with different sizes can potentially reduce the efficiency of DLD-based separation. In order to enhance the efficiency of separating CTCs clusters, Liu *et al.* designed U-shaped pillars in the microchannel, which combined the characteristics of conventional circular and I-shaped pillars to induce the rotation of asymmetrical CTCs clusters [55]. In the DLD cluster sorting session, a two-stage continuous sorting region was arranged, with critical diameters of 30 μm and 20 μm, respectively. This arrangement effectively disperses the displacement of target cells in these two distinct sorting regions. As shown in Fig. 2B, red circles highlight isolated 4T1 clusters, while red and blue striped regions represent the flow areas of blood samples entering and PBS buffer, respectively. Their results showed that 4T1 clusters can be efficiently rotated and isolated, which successfully recovered 88.58% of CTCs clusters with a purity of 92.20%.

2.1.3. Dielectrophoresis-based CTCs separation

DEP-based separation utilizes the disparities in electric properties of CTCs and normal blood cells to isolate CTCs from the biological samples. Under an electric field, the polarizing-induced dielectrophoretic forces acting on CTCs and normal blood cells are distinct. The CTCs experience a positive DEP force while the normal cells experience a negative force. Based on this, the CTCs and normal blood cells have different flow pathways in the microfluidic channel under an electric field generated from the electrodes located in the two sides of the chamber, and they can be collected from the different outlets [56,57].

Chiu *et al.* combined the DEP-based separation and laminar flow within a microfluidic system for the isolation of target CTCs [58]. When a cell suspension flowed through the primary microchannel, the target CTCs were identified and then selectively directed into the side microchannel for isolation. As a result, the microfluidic system achieved a capture efficiency of 41.5% for the human prostate cancer cell line. In another study, Li *et al.* reported a continuous and high-throughput capture of CTCs using arrays of wireless electrodes based on DEP [59]. The configuration of wireless electrode arrays simplifies the expansion of DEP devices in both the x and y directions. The alternating current field generated by the wireless electrode array enabled simultaneous CTCs capture across parallel microchannels. In addition, the authors also designed micro-holes embedded on the surface of the microchannel to provide discrete capture sites for individual cells and achieved a capture efficiency of over 80% for the MDA-MB-231 cells.

Arslan *et al.* introduced a microfluidic chip based on DEP for the isolation of CTCs by manipulating the frequency and magnitude of the alternating current [60]. As the schematic shown in Fig. 2C, the microfluidic chip comprised a microchannel with two inlets and two outlets, positioned above rectangular planar electrodes that were equally spaced and isolated. The microchannel and four rectangular electrodes were oriented at an angle of 13°. By applying a sinusoidal voltage of 10–12 Vpp at 1 MHz, MCF-7 breast cancer cells and normal blood cells were directed toward separate outlets. When 138 breast cancer cells were introduced into the main channel through the cell inlet, only 3 cancer cells exited through the outlet for blood cells, while 135 cancer cells were successfully enriched and exited through the CTCs outlet, demonstrating a CTCs enrichment efficiency of 98%.

DEP-based separation has demonstrated the ability to capture heterogeneous CTCs due to the distinct dielectric properties exhibited by different types of CTCs [61–64]. Chen *et al.* employed two established DEP-based separation strategies involving measuring dielectrophoretic responses of different cell types to obtain

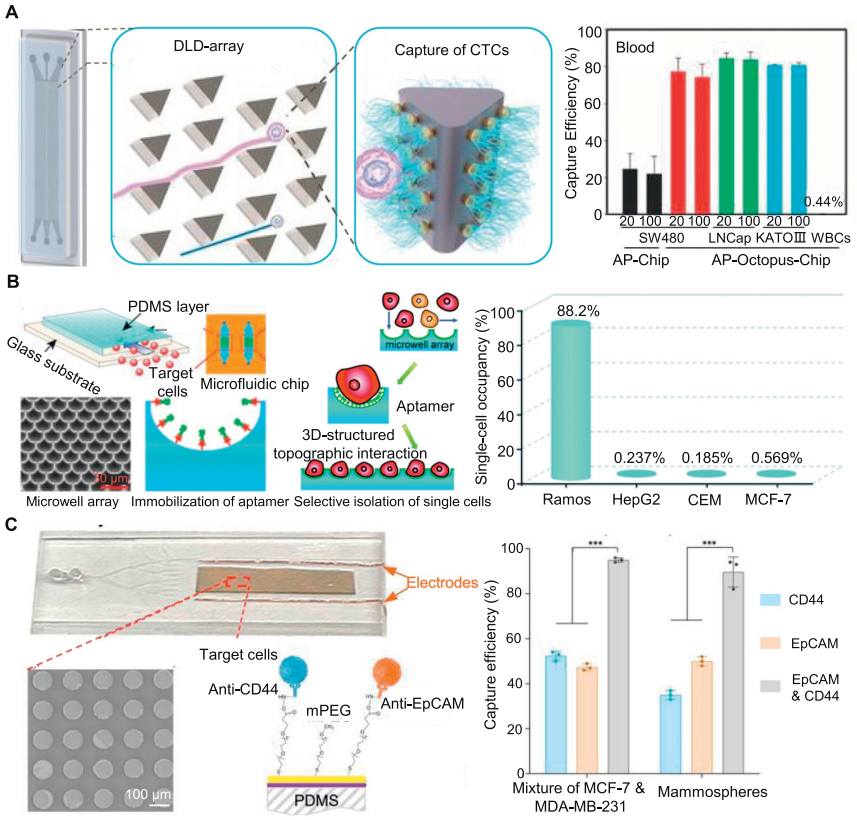

Fig. 3. Affinity-based microfluidic strategies for high-efficiency isolation of CTCs. (A) The schematic of the DLD-patterned microfluidic chip with multivalent aptamer functionalization for high-efficient capture of CTCs from the blood samples. The capture efficiency for the SW480, LNCaP, and KATO III. Reproduced with permission [72]. Copyright 2019, Wiley-VCH. (B) The schematic of the topological matching affinity interfaces in microfluidic chips for the isolation of CTCs, and capture efficiency of target Ramos compared to non-targeted HepG2, CEM, and MCF-7. Reproduced with permission [73]. Copyright 2012, The Royal Society of Chemistry. (C) A real picture and a SEM image of microfluidic system, and the schematic illustrations detailing the dual antibody functionalization targeting both CD44 and EpCAM, and the capture efficiency of microfluidic chip functionalized with dual antibody for a heterogeneous mixture of MCF-7 and MDA-MB-231 cancer cells, and mammospheres, compared with only anti-EpCAM and only anti-CD44 functionalized chips. Reproduced with permission [83]. Copyright 2022, American Chemical Society.

averaged DEP spectra and the distribution of dielectric properties within individual cell populations for the isolation of circulating melanoma cells [26]. Their experimental results show that the range of dielectric properties of peripheral blood mononuclear cells is more diverse among late-stage patients compared to healthy donors. After a series of screening evaluations, a frequency of 16 Vpp at 50 kHz was chosen as the optimal parameter, and the capture efficiency of 74% for circulating melanoma cells was achieved.

2.2. *Affinity-based strategies*

Physical force-based strategies rely on the distinct size, electrical property, and deformability between the blood cells and CTCs to realize the isolation of the CTCs. However, these approaches have limitations due to some degree of overlap in the size of CTCs and normal blood cells, which reduces the separation efficiency. To overcome this, affinity-based strategies exploit the unique proteins or molecules expressed by CTCs that are not typically found on normal blood cells but are associated with cancer cells. These strategies rely on highly specific interactions between the specific recognition molecules and the proteins of the target CTCs to select and accurately capture target CTCs from the complex biological fluid. The most commonly employed affinity-based strategy is the immobilization of the specific recognition molecules, such an antibodies [65], aptamers [66,67], and peptides [8,68], onto the surfaces of the microchannels and the micro-/nanostructures. In addition, the affinity-based strategy can also be combined with the physical-force based strategies to further improve the separation efficiency. Ahmed *et al.* developed a monovalent aptamer-based DLD microfluidics to capture SW480 efficiently and sensitively [51]. In their microfluidic chip, the triangular micropillars are rotated clockwise by 15° around their axis for providing a smoother gradient of hydrodynamic forces, ensuring that the CTCs can be frequently and extensively contact with the affinity molecule-modified micropillars. Based on the synergetic effect of fluid hydrodynamic and affinity, the authors obtained a capture efficiency of 92.2% for SW480 from the buffer solution. The monovalent modified aptamers exhibit strong affinity in buffer solutions, but their binding efficiency is compromised when employed in complex biological samples, thus resulting in the reduction of the capture efficiency [69].

Through creating multivalent recognition, the binding interactions between targets and recognition molecules on microfluidic affinity interfaces can be further enhanced, leading to improved capture efficiency of CTCs in complex biological fluids [70,71]. Song *et al.* modified the DLD-patterned microfluidic chip with multivalent aptamer-functionalized gold nanoparticles to enhance the efficiency of capturing CTCs [72]. As shown in Fig. 3A, the capture efficiencies of the multivalent aptamer-functionalized chip for SW480, LNCaP, and KATO III are more than 70% in the blood sample, which is significantly improved compared to the monovalent aptamer-modified chip with only 21.6%. Moreover, the affinity-based strategies can also be employed on microscale topographical structures that are comparable to the target CTCs for increasing the capture efficiency. As shown in Fig. 3B, Chen *et al.* developed an aptamer-encoded microwell for the isolation of individual tumor cells [73].

The microwell design promotes strong local topographical interactions between the three-dimensional features of CTCs and recognition molecules. As a result, optimizing the microwell size resulted in a substantial increase in single-cell occupancy rate, from 0.5% to 88.2%.

In addition to the modification of specific recognition molecules on the surfaces of the microchannels or micro-/nanostructures, another widely employed affinity-based strategy is the immunomagnetic separation that utilizes recognition molecule-modified magnetic nanoparticles to capture the target CTCs selectively and continuously [50,74,75]. Chang *et al.* developed an integrated microfluidic platform for capturing CTCs using immunomagnetic particles with anti-EpCAM modification [76]. Their results demonstrated an approximate 89% capture efficiency for MCF-7 cells ranging in size from 10 μm to 30 μm using antibody-modified immunomagnetic particles in the microfluidic chip. To further enhance the magnetic trapping force, Chen *et al.* used the dynamic immunoaffinity interface within a herringbone chip to facilitate the isolation of the target CTCs [77]. The dynamic immunoaffinity interface enables frequent interaction between the CTCs and antibody-modified magnetic nanoparticles, gradually enhancing the magnetic trapping force, which resulted in the capture efficiency of 96.5% for the captured SW480 exhibiting EpCAM expression from blood samples. Such a high capture efficiency is increased by 115.8% and 491.4% compared to static immunoaffinity interface within the microfluidic chip and magnetic separation within the tubing, respectively.

The process of epithelial-mesenchymal transition (EMT) during tumor progression can lead to approximately 26.2% of castration-resistant prostate cancer patients exhibiting EpCAM-negative results in CTCs isolation [78–80]. This poses a challenge in capturing the target CTCs, making the isolation process more complicated and difficult. To address this issue, Yin *et al.* developed a microfluidic device functionalized with dual antibodies PSMA and EpCAM to capture the heterogeneous of CTCs [81]. The device consists of antibody and magnetic bead-functionalized Ni micropillar and herringbone structures. When the target cells changed from LnCAP to LnCAP-EMT, the capture efficiency of the single EpCAM antibody-modified chip decreased from 73.8% to 38.1%. In contrast, the dual antibodies modified chip significantly improved the capture efficiency to more than 85.0%. In another study, Wang *et al.* prepared fluorescent-magnetic nanoparticles that were modified with dual antibodies targeting EpCAM and N-cadherin to isolate and identify heterogeneous CTCs from the blood samples [82]. The dual antibodies modified magnetic nanoparticles demonstrate a capture efficiency of 99% and 81% for MCF-7 and HeLa, respectively. In comparison, the only anti-N-cadherin-modified nanoparticles exhibit limited isolation performance for the two cell types, with a capture efficiency of 17% for MCF-7 and 73% for HeLa. Kwizera *et al.* developed a microfluidic chip using electromicrofluidic technology and thiol-Au chemistry to efficiently capture heterogeneous CTCs expressing EpCAM+ and CD44+ [83]. The chip features two inlets and five consecutive bifurcating structures. As shown in Fig. 3C, the capture surfaces were initially coated with a titanium and gold film (with the thickness of 4 nm and 10 nm, respectively), subsequently adorned with methoxy–PEG (mPEG) and capture antibodies anti-CD44 and anti-EpCAM. The electric microfluidic chip controls cell movement between capture and non-capture regions by modulating the duration of the alternating electric field, achieving a 95% capture efficiency for a heterogeneous mixture of MCF-7 and MDA-MB-231 cancer cells, and a 90% capture efficiency for mammospheres. In contrast, the use of either anti-EpCAM or anti-CD44 alone on the modified capture surfaces resulted in diminished isolation performance, with respective capture efficiency of 35% and 50% for mammospheres, respectively. Therefore, modification of the microchannels with the dual antibodies can significantly improve the capture efficiency of heterogeneous CTCs.

Besides the affinity-based strategies that rely on positive tumor cell markers, CTCs can also be negatively selected based on blood cell-specific surface markers. One universal technique for WBC removal is the application of CD45 antibody-labeled microparticles, which selectively bind to and remove WBCs while leaving behind CTCs. Wang *et al.* developed a wedge-shaped microfluidic chip for negative selection of CTCs [84]. The microfluidic chip, with a maximum height of 60 μm and a minimum height of 5 μm, was used to exclude most blood cells. Microparticles modified with anti-CD45 antibody were introduced into the chip. As a result of using the wedge-shaped microfluidic chip, approximately 94.9% MCF-7 cells were captured in the chip. The advantage of negative selection over positive selection is its ability to collect all CTCs regardless of their surface marker expression, allowing for the retention of heterogeneous CTCs. However, one defect of the negative selection method is that not all nucleated cells in the blood express CD45, and the high concentration of WBCs in blood makes a lower purity of the isolated CTCs sample.

3. High-purity isolation of CTCs

The use of physical force-based strategies can significantly improve the capture efficiency of the CTCs from the biological fluid. However, the nonspecific attachment of contaminated components, especially WBCs, leads to a reduction in the purity of isolated CTCs and compromises the accuracy of subsequent molecular analysis. Hence, the development of microfluidic-based strategies designed to avoid the non-specific adhesion of blood cells and achieve the high-purity CTCs isolation becomes a matter of pressing importance. Until now, various surface modification strategies have been proposed for the functionalization of the microchannel surface to enhance their anti-adhesion properties and improve the purity of CTCs isolation. Such strategies include surface topographical micro-/nanostructures construction, chemical modification strategies, and biological modification strategies.

3.1. Surface topographical micro-/nanostructures design

Surface topographical micro-/nanostructures, deliberately designed to match the dimensions of CTCs, serve a dual purpose in facilitating the selective capture of target CTCs while reducing the nonspecific adhesion of WBCs. This strategy enables the high-purity isolation of CTCs by implementing appropriate topographical micro-/nanostructures on the surfaces of microchannels. Hui *et al.* developed a microfluidic chip integrated with an ivy-like hierarchical roughened zinc oxide (ZnO) nanograss surface for capturing CTCs with high-purity [85]. Fig. 4A shows the fabrication processes of the construction of ZnO nanograsses. The ivy-like hierarchical roughness of the ZnO nanograss surface promotes interactions with CTCs while minimizing the adhesion of WBCs. The capture efficiencies of CTCs on surfaces with and without ZnO nanograss coating show that there was no statistically significant difference in capture efficiency, while the number of non-specific adhesions of WBCs decreased from approximately 200 to less than 50, indicating that the ZnO nanograss surface effectively reduces the adhesion of WBCs while maintaining the capture efficiency of CTCs. Jiang *et al.* developed a platform with a nanocage-featured structure for the high-purity capture of CTCs [86]. The specific topological structure of the platform matched the filopodia of CTCs, resulting in a stronger adhesion force toward MCF-7 cells compared to peripheral blood mononuclear cells (PBMCs). As a result, the capture efficiency for MCF-7 cells reached 92%, and the non-specific adhesion of PBMCs was below 1%.

Given the significance of high-purity recovered CTCs for *ex vivo* culture and downstream analysis, Cheng *et al.* utilized a three-dimensional macro-porous PDMS channel with incorporated

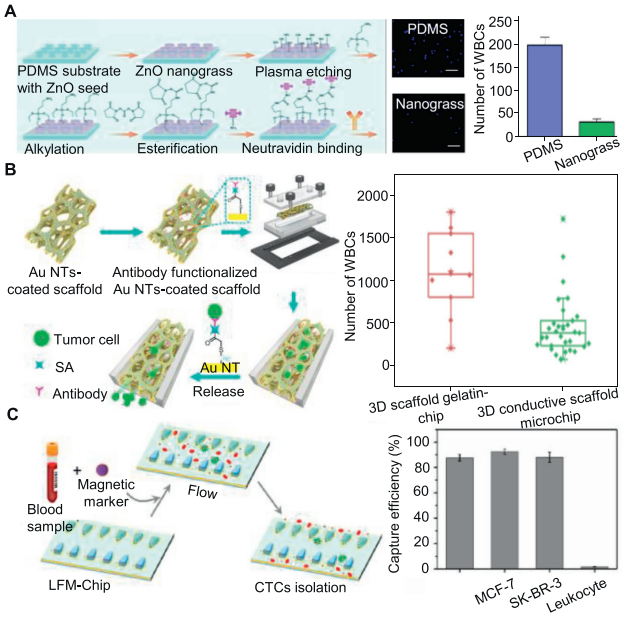

Fig. 4. Design of topographical micro-/nanostructures in microfluidics chips for high-purity isolation of CTCs. (A) Schematic of the fabrication of ivy-like hierarchical roughened ZnO nanograss surface within the microfluidic chip, accompanied by fluorescent images and the number of the nonspecific adhesion of WBCs on surfaces with and without the ivy-like ZnO nanograss coating. Reproduced with permission [85]. Copyright 2018, American Chemical Society. (B) 3D conductive scaffold microchip that relies on macroporous PDMS and incorporated antibody-modified gold nanotubes for high-purity capture of CTCs, and the number of WBCs on the 3D scaffold gelatin-chip and 3D conductive scaffold microchip. Reproduced with permission [87]. Copyright 2021, American Chemical Society. (C) Schematic diagram showing the LFM chip for isolation of CTCs and capture efficiencies to MDA-MB-231, MCF-7, SK-BR-3, and leukocyte. Reproduced with permission [40]. Copyright 2023, American Chemical Society.

antibody-modified Au nanotubes on the PDMS surface for the capture of CTCs with high purity (Fig. 4B) [87]. The macro-porous structure induces a transition of fluid flow behavior from laminar flow to chaotic flow, effectively increasing the contact frequency between the capturing agent and the target CTCs. Their results show that the Au nanotube coating on the 3D scaffold exhibits excellent conductivity. Under voltage applied, the Au-S bonds were broken, and the captured CTCs can be selectively released through electrochemical stimulation, while non-specifically bound WBCs do not release in this process. This targeted release mechanism enhances the retrieval of high-purity CTCs, demonstrated by the presence of only 460 WBCs observed, compared to 1100 when using a gelatin layer without any selectivity. Lv *et al.* employed the size-selective lateral flow microarray (LFM) integrated with a gold nanorod pre-embedded gelatin (NIR-responsive hydrogel) capture unit to achieve high-purity capture and site-specific release of single CTCs for investigating their heterogeneity (Fig. 4C) [40]. The LFM chip consists of a main channel and two side channels, with the main channel responsible for capturing CTCs and the side channel for minimizing the WBCs adhesion. By controlling the size of the capture structure within the LFM chip through adjustments in the mass fraction and number of hydrogel layers, the authors obtained a capture efficiency reached 88% for MCF-7 cells, with only 1.7% of WBCs non-specifically adhered.

3.2. Surface chemical modification strategies

Surface chemical modification strategies involve modifying the surfaces of the microchannel with anti-adhesive molecules to reduce non-specific interactions between the surfaces and the blood cells, achieving the goal of repelling the adhesion of WBCs [88–90]. The commonly used anti-adhesive molecules include bovine serum albumin (BSA) [91], polyethylene glycol (PEG) [88,92], zwitterionic polymers [93], *etc.* Ding *et al.* utilized BSA as a linker on the capture surfaces to alleviate non-specific adhesion of WBCs [94]. Their results show that approximately 50%–70% of spiked MCF-7 cells were successfully captured from a solution containing 1×10^6 WBCs, with the non-specifically adhered WBCs less than 0.1%. Li *et al.* modified the microchannel with PEG, and affinity molecules to create a surface for high-purity capture of CTCs [93]. This surface modification strategy resulted in a capture efficiency of 91%, with contaminated WBCs less than 0.001%.

Xiao *et al.* improved the purity of capturing CTCs by introducing zwitterionic poly(2-methacryloyloxyethyl phosphorylcholine) (PMPC) and folate (FA) onto polyethyleneimine (PEI)/polyvinyl alcohol (PVA) nanofibers within a microfluidic chip (Fig. 5A) [95]. The presence of FA on the capture surface facilitated highly specific and efficient capture of CTCs expressing the FA receptor, while the immobilization of PMPC on the capture surface endowed it with the antiadhesive properties against normal blood cells, which significantly elevated the purity of the captured CTCs. Using this fiber-integrated microfluidic platform, they achieved highly efficient capture of FA receptor-expressing cancer cells, such as KB, HeLa, and SKOV-3 cells, with capture efficiencies ranging from 92.3% to 93.5% at a flow rate of 2 mL/h. Furthermore, only a few WBCs are non-specifically attached on the capture surface under the static conditions. Likewise, they utilized hyaluronic acid (HA)-functionalized electrospun chitosan nanofibers (CNFs) and embedded in a microfluidic chip to specifically capture the CTCs that overexpressed CD44 (Fig. 5B) [96]. To reduce the nonspecific adhesion of WBCs, zwitterionic carboxyl betaine acrylamide (CBAA) was also grafted onto the electrospun CNFs. HA-functionalized electrospun CNFs with CBAA modification demonstrated a capture efficiency of 81% for A549 cells. Additionally, the nonspecific adhesion of WBCs was significantly reduced to only 0.17%, representing a 21-fold reduction compared to the electrospun CNFs without CBAA modification.

Wu *et al.* reported a green liquid-like interface design strategy to capture CTCs with high purity (Fig. 5C) [38]. The linear PDMS polymer brushes were grafted on the surfaces using a covalent layer-by-layer assembly and biotinylated anti-EpCAM modification processes in non-toxic solutions. Due to the high mobility of the PDMS brushes at room temperature, the modified surfaces exhibited slippery properties for various polar and non-polar liquids, similar to that of the fluids [68,97]. Meanwhile, the liquid-like polymer brushes can also minimize the interactions between the WBCs and the modified surfaces. Thereby significantly reduced non-specific adhesion of WBCs shown in the SEM images demonstrates the excellent anti-adhesion property of the liquid-like molecule modified surface. To prove their potential for high-purity capture of CTCs, the authors modified the DLD microchannels with the liquid-like molecules and the anti-EpCAM antibody to capture the target CTCs from the whole blood. Experimental results show the nonspecific adhered WBCs were less than 0.14% in the DLD chip with liquid-like molecule and anti-EpCAM modification, which is a 5.7-fold reduction compared to the DLD-chip with only anti-EpCAM modification.

3.3. Surface biological modification strategies

Surface biological modification strategies employ endogenous biomolecules as camouflage coatings to hinder the non-specific adhesion of WBCs [98,99]. One effective method in these strategies is the use of a lipid bilayer, which serves as a proficient means of disguising homologous cells [100,101]. In the bloodstream, homologous WBCs do not form clusters within the circulation, and

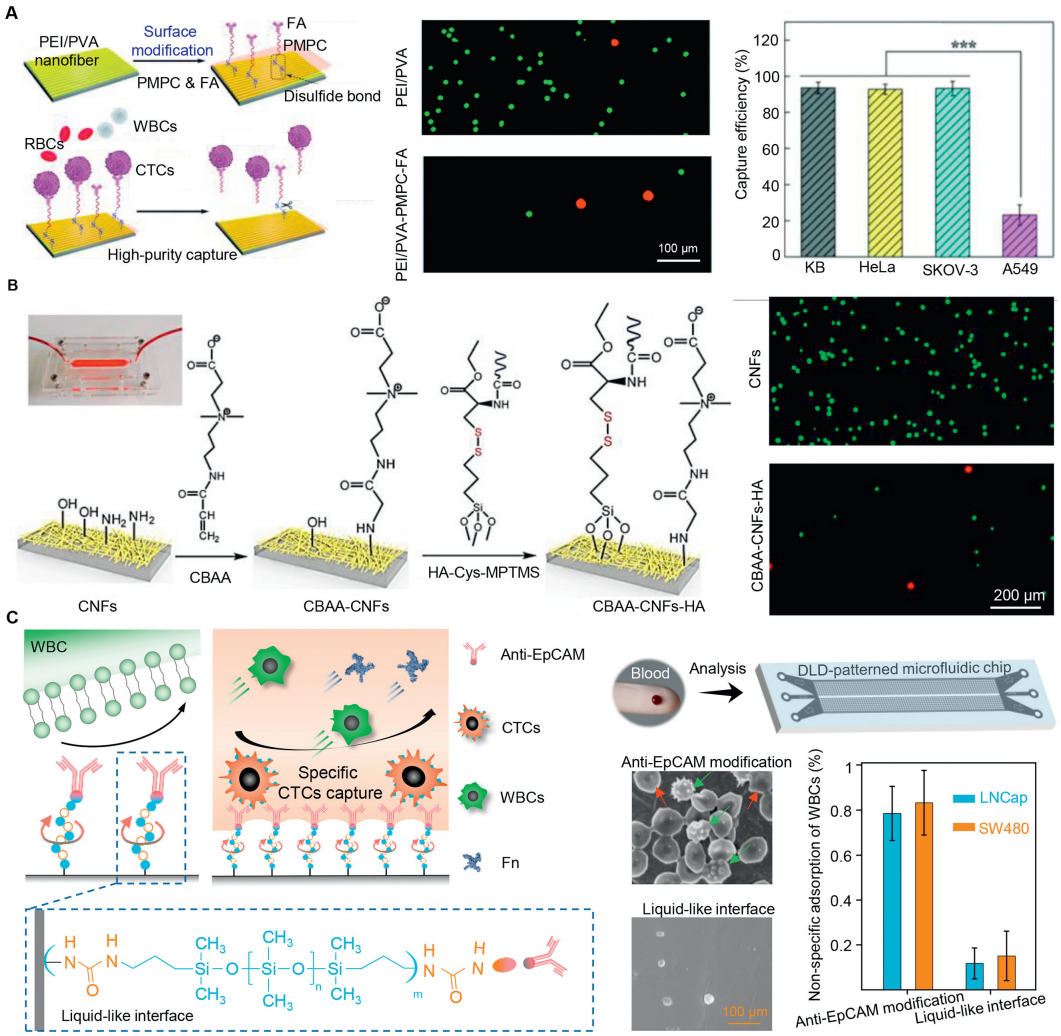

Fig. 5. Surface chemical modification strategies for high-purity capture of CTCs in microfluidic chips. (A) The schematic of modification processes of the PEI/PVA nanofibrous with PMPC and FA modification to improve the purity of captured CTCs. Fluorescence microscopic images of HeLa cells (green) and WBCs (red) captured by PEI/PVA nanofibrous with and without PMPC and FA modification and capture efficiency of KB, HeLa, SKOV-3, A549 in the microfluidic chip modified by PEI/PVA-PMPC-FA nanofibers. Reproduced with permission [95]. Copyright 2018, The Royal Society of Chemistry. (B) Schematic of the fabrication of HA-functionalized electrospun CNFs with CBAA modification within the microfluidic chip. Fluorescence microscopic images of A549 cells and WBCs captured by electrospun CNFs, and HA-functionalized electrospun CNFs with CBAA modification under static conditions. Reproduced with permission [96]. Copyright 2018, American Chemical Society. (C) Schematic illustration of the mechanism of specific capture of CTCs and reduction of non-specific adhesion of proteins and WBCs on the surfaces modified by liquid-like PDMS brushes and anti-EpCAM. SEM images show the WBCs (indicated by green arrow) and RBCs (indicated by red arrow) on the surface modified by PDMS brushes and surfaces modified by only anti-EpCAM. Statistical results of the nonspecific adherence of WBCs on micropillar surfaces within DLD-chips with and without PDMS brushes modifications. Reproduced with permission [38]. Copyright 2024, Chinese Chemical Society.

platelets (PLTs) can recognize and interact with CTCs, enabling them to effectively discern both CTCs and WBCs [102,103].

Rao *et al.* modified the immunomagnetic beads with PLT-WBC hybrid membranes to isolate the CTCs [104]. Through these biological modifications, the authors realized the capture efficiency of 91.77% for MCF-7 with purity of 96.98%, which is significantly improved compared to the commercial immunomagnetic beads only with capture efficiency of 66.68% and purity of 66.53%. Zhang *et al.* modified the magnetic nanoclusters camouflaged by leukocyte membrane in a nickel-patterned microfluidic device to achieve fast and accurate separation of CTCs from whole blood with reduced non-specific adhesion of normal blood cells (Fig. 6A) [105]. The leukocyte membrane camouflage not only suppressed the non-specific binding of WBCs but also facilitated the anchoring of SYL3C aptamers. The results of their study demonstrated that over 90% of MCF-7, 4T1, and MDA-MB-231 cells could be captured from whole blood within 20 min, with almost no nonspecific adhesion of control cells as Jurkat and J774A.1.

Another critical feature of biological membrane interfaces is dynamic lateral fluidity, allowing rearrangement and positioning of membrane-binding components during multivalent ligand-receptor interactions. Wu *et al.* developed a fluidic aptamer-functionalized soft and high-affinity nanointerface microfluidic chip (FLASH-Chip) for high purity CTCs separation [33]. As shown in Fig. 6B, the FLASH-Chip was built by grafting the aptamer-functionalized leukocyte membrane nanovesicles on the DLD arrays. The natural adaptability of leukocyte membrane interfaces enables recognition ligands to rearrange, promoting high-affinity binding and synergistic multivalent targeting post-binding. Meanwhile, the anticytolytic properties of the leukocyte membrane significantly can reduce the nonspecific adhesion of normal blood cells. Compared to single-valent functionalized chips (labeled as Apt-Chip), this fluidic nanointerface achieved a 4-order magnitude improvement in aptamer affinity and a 7-fold increase in blood capture rate. After introducing 10^6 WBCs into the FLASH-Chip, only approximately 260 cells remained. In comparison, the Apt-Chip non-specifically

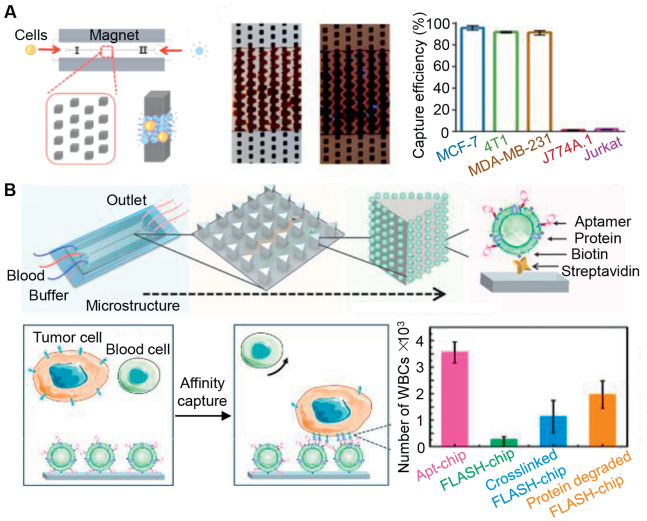

Fig. 6. Surface biological modification strategies for high-purity capture of CTCs in microfluidic chips. (A) A schematic of combining magnetic nanoclusters camouflaged by leukocyte membrane with a nickel-patterned microfluidic device for the isolation of CTCs. Microscopy images of MCF-7 cells captured by the nickel square array composed of magnetic nanoclusters. Capture efficiencies of MCF-7, 4T1, MDA-MB-231, Jurkat T, and J774A.1 with leukocyte membrane fragments modified the magnetic nanoclusters in a microfluidic chip. Reproduced with permission [105]. Copyright 2019, American Chemical Society. (B) A schematic of the FLASH-Chip with leukocyte membrane nanovesicles modifications to reduce nonspecific adsorption of WBCs and CTCs isolation. The quantification of residual WBCs in Apt-chip, FLASH-Chip, crosslinked FLASH-Chip (where the nanointerface was crosslinked), protein degraded FLASH-Chip (with membrane proteins digested using trypsin). Reproduced with permission [33]. Copyright 2020, American Chemical Society.

captured more than 3500 WBCs. Shen *et al.* reported the use of RBCs membrane as functional coating for antibody grafting to realize high-purity capture of CTCs in DLD microfluidic chips (RBC-Chip) [16]. The molecular clustering based on lateral mobility of cell membranes allowed for enhanced affinity recognition, resulting in high-performance capture of SW480 with efficiency of 94.0%, slightly higher than the 84.1% achieved with microfluidic chip without RBCs membrane modification (SI-chip). Meanwhile, the anti-adhesive properties of the RBCs membrane significantly contributed to the high purity of isolated CTCs. The non-specific adsorption of two control cells, CCRF-CEM and Jurkat, on the RBC-Chip was only 0.35% and 0.45%, respectively, significantly lower than the 6.7% and 6.8% observed on the SI-Chip.

4. Summary and outlook

In this review, we discussed the recent advancement of the microfluidic-based strategies for high-efficiency and high-purity isolation of CTCs. Through the rational design of the microchannel geometry and the micro-/nanostructures construction [106,107], the CTCs can be effectively separated from the biological samples. In addition, physical/chemical affinity design on the microchannel surfaces can further improve the capture efficiency and selectivity [108,109]. Moreover, the surface modifications of the microchannels can be adopted for the reduction of the non-specific adhesion of the contaminated components to isolate CTCs with high purity [110]. Table 1 summarizes the capture efficiency and purity of CTCs isolation based on microfluidic-based strategies developed in recent years. With the advantage of low sample consumption, rapid and continuous processing, gentle and efficient cell handling, low cost, *etc.*, microfluidic technology provides a powerful and versatile strategy for the high-efficiency and high-purity isolation of CTCs

Table 1
Comparison of microfluidic-based strategies for isolation CTCs in terms of purity and efficiency.

Micro/ nanostructure	Modification	Capture efficiency	Capture purity (adhesion of WBCs)	Refs.	Publication year
Stepped structures	–	54% (T24) 69% (A375)	0.02%–0.6%	[106]	2016
Lateral filter arrays	Anti-EpCAM	88.5% (L3.6pl)	0.36%	[44]	2019
Triangle pillar arrays	Anti-EpCAM	99.9%(SW480) 20.3% (293T)	0.005%	[51]	2017
Si nanopillars	Anti-EpCAM	>95% (MCF-7, PC3, T24)	–	[107]	2011
ZnO nanograss	Anti-EpCAM	85.47% (MCF-7) 66.53% (Bxpc3) 11.9% (HeLa)	–	[85]	2018
Triangle pillar arrays	Tetrahedral DNA nanostructures (TDN) with SYL3C modification	85.4% (MCF-7) 73% (SW480) 13.5% (Ramos)	0.36%	[69]	2020
Silicon nanowires	Magnetic nanocomposites with anti-EpCAM modification	90.3% (MCF-7)	–	[108]	2017
NanoGold	TDN with anti-EpCAM modification	91.3 % (HNSCC)	–	[109]	2023
Porous poly-dimethylsiloxane	Au nanotubes with anti-EpCAM modification	92.8% (MCF-7)	0.07%–1.721%	[87]	2021
Lateral flow arrays	Gold nanorod with anti-EpCAM modification	88% (MCF-7)	1.7%	[40]	2022
Nanofibers	Carboxyl betaine acrylamide with hyaluronic acid modification	81% (A549)	0.17%	[96]	2018
Nanofibers	Poly(2-methacryloyloxyethyl phosphorylcholine) with arginine-glycine-aspartic acid peptide modification	79.3% (A549)	0.0811%	[110]	2018
Nanofibers	Poly(2-methacryloyloxyethyl phosphorylcholine) with hyaluronic acid modification	92.3%–93.5% (KB, HeLa, SKOV-3)	–	[95]	2018
Triangle pillar arrays	Au nanoparticles with SYL3C modification	74.2%–84.4% (SW480, LNCap, KATO III)	0.44%	[72]	2019
Magnetic beads	Hyaluronic acid	89.5% (HeLa) 13.8% (L929)	–	[74]	2022
Triangle pillar arrays	PDMS polymer brush with anti-EpCAM modification	>70% (LNCap, SW480)	0.16%	[38]	2023
Magnetic nanoclusters	Leukocyte membrane coating with SYL3C modification	91% (MCF-7)	–	[105]	2019
Triangle pillar arrays	Leukocyte membrane surface with SYL3C modification	91.2% (SW480) 82.1% (HCT 116)	0.026%	[33]	2020
Triangle pillar arrays	RBCs membrane surface with anti-EpCAM modification	96.5% (SW480) 35.3% (A549)	0.0086%–0.1049%	[16]	2022

and further downstream operation, such as molecular analysis, genetic profiling, drug sensitivity testing, and studying metastatic potential.

Despite significant advancements in microfluidic-based strategies for isolating CTCs, achieving both high efficiency and high purity simultaneously remains a challenge. Surface modification of affinity molecules has shown promise in improving the capture efficiency and specificity for target CTCs in biological samples. However, these modified affinity molecules have limitations in reducing non-specific adhesion of contaminants such as WBCs and proteins. Therefore, the surface modification of anti-adhesive molecules is necessary to improve capture purity. Nevertheless, the modification of anti-adhesive molecules often leads to a decrease in capture efficiency, possibly due to their anti-adhesive properties affecting the target CTCs to some extent. Microfluidic chips modified with biological molecules, such as WBC and RBC membranes, have demonstrated excellent performance in CTCs isolation with both high efficiency and high purity. However, the modification of these biomolecules necessitates sophisticated processes and strict requirements in specialized biological laboratories, making it unsuitable for conventional chemical or biological labs [33,111]. To address this, the synthesis and modification of bio-inspired molecules with properties similar to biomolecules, such as dynamic lateral fluidity, in a simpler operation process in conventional laboratories show great potential to improve capture efficiency and purity. Building upon successful bio-inspired molecule modifications, further grafting of affinity molecules, such as multi-valence or multiple affinity molecules, can enhance efficiency and selectivity.

The detection, enumeration, and characterization of CTCs have demonstrated significant potential in the clinical applications of early-stage invasive cancer detection, treatment selection, drug resistance identification, and the identification of new therapeutic targets. Despite the successful capture of CTCs using various physical-force and affinity-based strategies through microfluidic technology, the studies are still needed to optimize CTCs isolation performance, including high efficiency and high purity. Moreover, the viability of captured CTCs is also crucial for enabling a wide range of downstream analyses that can provide critical insights into cancer biology and patient-specific tumor characteristics. Therefore, prioritizing green and non-toxic molecular modifications that are cell-friendly is crucial. By harnessing the synergistic effect of physical-force and affinity-based strategies, we believe that the microfluidic technologies can provide effective information on cancer progression and metastasis, thereby paving the way for breakthroughs in personalized cancer therapy, diagnosis, prognosis, and screening of multiple anti-metastatic drugs for cancer patients.

Declaration of competing interest

The authors declare that they have no known competing financial interests or personal relationships that could have appeared to influence the work reported in this paper.

Acknowledgments

This work was supported by the National Natural Science Foundation of China (Nos. 52025132, 22005255, 21975209, 21621091, 22021001, T2241022), the National Science Foundation of Fujian Province of China (No. 2022J02059), the Fundamental Research Funds for the Central Universities of China (No. 20720220085), the 111 Project (Nos. B17027, B16029), the Science and Technology Projects of Innovation Laboratory for Sciences and Technologies of Energy Materials of Fujian Province (No. RD2022070601), the New Cornerstone Science Foundation through the XPLORER PRIZE.

References

[1] I. Soerjomataram, F. Bray, Nat. Rev. Clin. Oncol. 18 (2021) 663–672.
[2] H. Rumgay, K. Shield, H. Charvat, et al., Lancet Oncol. 22 (2021) 1071–1080.
[3] S. Regmi, C. Poudel, R. Adhikari, K.Q. Luo, Biosensors 12 (2022) 459.
[4] Y. Wu, Y. Zhou, R. Paul, et al., Anal. Chem. 94 (2022) 12159–12166.
[5] J. Chen, H. Wang, L. Zhou, et al., Lab. Anal. 36 (2022) e24341.
[6] H. Yu, C. Yang, Q. Tai, M. Gao, X. Zhang, Anal. Chem. 95 (2023) 5232–5239.
[7] D. Crosby, S. Bhatia, K.M. Brindle, et al., Science 375 (2022) eaay9040.
[8] R. Han, Y. Li, M. Chen, et al., Anal. Chem. 94 (2022) 2204–2211.
[9] R. Lawrence, M. Watters, C.R. Davies, K. Pantel, Y.J. Lu, Nat. Rev. Clin. Oncol. 20 (2023) 487–500.
[10] F. Chemi, S. Mohan, T. Guevara, et al., Front. Oncol. 11 (2021) 672195.
[11] M. Zhao, D. Mi, B.E. Ferdows, et al., Nano Today 42 (2022) 101361.
[12] Y. Yin, Y.P. Yan, B. Fan, et al., Research 6 (2023) 14.
[13] H. Ye, K. Wang, Q. Lu, et al., Biomaterials 242 (2020) 119932.
[14] K. Shirai, G. Guan, T. Meihui, et al., Lab Chip 22 (2022) 4418–4429.
[15] B. Dou, L. Xu, B. Jiang, R. Yuan, Y. Xiang, Anal. Chem. 91 (2019) 10792–10799.
[16] H. Shen, R. Su, J. Peng, et al., Bioact. Mater. 11 (2022) 32–40.
[17] K. Kang, X. Zhou, Y. Zhang, et al., Small 17 (2021) 2007796.
[18] J. Yin, J. Deng, L. Wang, et al., Anal. Chem. 92 (2020) 6968–6976.
[19] Q. Huang, F.B. Wang, C.H. Yuan, et al., Theranostics 8 (2018) 1624.
[20] B. Wang, S. Zhang, J. Meng, et al., Adv. Mater. 33 (2021) 2103999.
[21] W. Jiang, L. Han, G. Li, et al., Acta Biomater. 162 (2023) 226–239.
[22] Y. Yu, Y. Zhang, Y. Chen, et al., ACS Sens. 8 (2023) 1858–1866.
[23] Y. Liu, H. Shen, X. Yang, et al., TrAC Trends Anal. Chem. 3 (2022) 116894.
[24] J. Wang, W. Lu, C. Tang, et al., Anal. Chem. 87 (2015) 11893–11900.
[25] E.S. Park, C. Jin, Q. Guo, et al., Small 12 (2016) 1909–1919.
[26] H. Chen, S.Y. Osman, D.L. Moose, et al., Lab Chip 23 (2023) 2586–2600.
[27] L. Sha, W. Wang, Q. Liu, et al., Anal. Chim. Acta 1274 (2023) 341556.
[28] S. Wang, X. Yang, F. Wu, et al., Small 16 (2020) 1905318.
[29] T. Chen, C. Huang, Y. Wang, J. Wu, Chin. Chem. Lett. 33 (2022) 1180–1192.
[30] L. Menze, P.A. Duarte, L. Haddon, M. Chu, J. Chen, ACS Nano 16 (2022) 211–220.
[31] S. Wang, R. Zhou, Y. Hou, M. Wang, X. Hou, Chin. Chem. Lett. 33 (2022) 3650–3656.
[32] S. Qiu, C. Shen, X. Jian, et al., Chin. Chem. Lett. 33 (2022) 2701–2704.
[33] L. Wu, H. Ding, X. Qu, et al., J. Am. Chem. Soc. 142 (2020) 4800–4806.
[34] Z. Sheng, X. Liu, L. Min, et al., Chin. Chem. Lett. 28 (2017) 1131–1134.
[35] F. Wu, S. Chen, B. Chen, et al., Small 14 (2018) 1702170.
[36] F. Wu, J. Li, K. Zhang, et al., ACS Appl. Mater. Interfaces 8 (2016) 109–121.
[37] N. Sun, M. Liu, J. Wang, et al., Small 12 (2016) 5090–5097.
[38] F. Wu, X. Chen, S. Wang, et al., CCS Chem. 6 (2024) 507–517.
[39] Y. Wu, A.G. Stewart, P.V.S. Lee, Lab Chip 21 (2021) 2812–2824.
[40] S. Lv, D. Zheng, Z. Chen, et al., Anal. Chem. 95 (2022) 1201–1209.
[41] W. Geng, Y. Liu, N. Yu, et al., Anal. Chim. Acta 1255 (2023) 341138.
[42] M.S. Islam, X. Chen, Biotechnol. Prog. 5 (2023) e3341.
[43] M. Hosokawa, T. Hayata, Y. Fukuda, et al., Anal. Chem. 82 (2010) 6629–6635.
[44] K. Chen, P. Dopico, J. Varillas, et al., Angew. Chem. 131 (2019) 7688–7692.
[45] Y. Zhang, Z. Wang, L. Wu, et al., Small 14 (2018) 1704433.
[46] X.F. Zhang, X. Lu, W.L. Gao, et al., Transl. Oncol. 14 (2021) 100959.
[47] M. Boya, T. Ozkaya-Ahmadov, B.E. Swain, et al., Nat. Commun. 13 (2022) 3385.
[48] R. Gao, L. Cheng, S. Wang, et al., Talanta 207 (2020) 120261.
[49] R. Nasiri, A. Shamloo, S. Ahadian, et al., Small 16 (2020) 2000171.
[50] D. Qiao, H. Li, W. Zhu, et al., Chin. Chem. Lett. 35 (2024) 108646.
[51] M.G. Ahmed, M.F. Abate, Y. Song, et al., Angew. Chem. Int. Ed. 56 (2017) 10681–10685.
[52] Z.B. Liu, Y.Q. Huang, W.L. Liang, et al., Lab Chip 21 (2021) 2881–2891.
[53] S.H. Au, J. Edd, A.E. Stoddard, et al., Sci. Rep. 7 (2017) 2433.
[54] Z. Liu, R. Chen, Y. Li, et al., Adv. Biosyst. 2 (2018) 1800200.
[55] S.J. Huang, C.M. Chang, Y.T. Lu, C.H. Liu, Sens. Actuators B 394 (2023) 134369.
[56] K. Zhao, P. Zhao, J. Dong, et al., Biosensors 12 (2022) 757.
[57] B.G. Hawkins, N. Lai, D.S. Clague, Micromachines 11 (2020) 391.
[58] T.K. Chiu, W.P. Chou, S.B. Huang, et al., Sci. Rep. 6 (2016) 32851.
[59] M. Li, R.K. Anand, J. Am. Chem. Soc. 139 (2017) 8950–8959.
[60] Z. Çağlayan Arslan, Y. Demircan Yalçın, H. Külah, Electrophoresis 43 (2022) 1531–1544.
[61] E.A. Henslee, M.B. Sano, A.D. Rojas, E.M. Schmelz, R.V. Davalos, Electrophoresis 32 (2011) 2523–2529.
[62] A. Ur Rehman, R.S. Zabibah, S. Kharratian, A. Mustafa, J. Visualized Exp. 186 (2022) e63850.
[63] T.R. Szymborski, M. Czaplicka, A.B. Nowicka, et al., Biosensors 12 (2022) 681.
[64] N. Alinezhadbalalami, T.A. Douglas, N. Balani, S.S. Verbridge, R.V. Davalos, Electrophoresis 40 (2019) 2592–2600.
[65] D. Cetin, M. Okan, E. Bat, H. Kulah, Colloids Surf. B 188 (2020) 110808.
[66] D. Wang, J. Wang, Y. Wang, et al., Chem. Sci. 13 (2022) 10395–10405.
[67] C. Liao, Z. Wu, C. Lin, et al., Smart Medicine 2 (2023) e20220020.
[68] M. Bai, X. Tian, Z. Wang, et al., Anal. Chem. 95 (2023) 5307–5315.
[69] J. Zhang, B. Lin, L. Wu, et al., Angew. Chem. 132 (2020) 14219–14223.
[70] Q. Li, Y. Wang, W. Gao, et al., Talanta 266 (2024) 125007.
[71] T.L. Lee, S.C. Huang, C.C. Huang, et al., Carbon 216 (2024) 118576.
[72] Y. Song, Y. Shi, M. Huang, et al., Angew. Chem. Int. Ed. 58 (2019) 2236–2240.
[73] Q. Chen, J. Wu, Y. Zhang, Z. Lin, J.M. Lin, Lab Chip 12 (2012) 5180–5185.
[74] D. Yin, A. Shi, B. Zhou, et al., Langmuir 38 (2022) 11080–11086.
[75] Y. Zuo, Y. Xia, W. Lu, et al., Nanoscale 15 (2023) 3872–3883.
[76] C. Chang, W. Huang, S.I. Jalal, et al., Lab Chip 15 (2015) 1677–1688.

[77] X. Chen, H. Ding, D. Zhang, et al., Adv. Sci. 8 (2021) 2102070.
[78] B. Kwak, J. Lee, J. Lee, et al., Biosens. Bioelectron. 101 (2018) 311–316.
[79] Q. Li, Y. Wang, W. Gao, et al., Talanta 6 (2023) 125007.
[80] Y. Xu, B. Chen, M. He, Z. Cui, B. Hu, Anal. Chem. 95 (2023) 14061–14067.
[81] C. Yin, Y. Wang, J. Ji, et al., Anal. Chem. 90 (2018) 3744–3751.
[82] Z. Wang, N. Sun, H. Liu, et al., ACS Appl. Mater. Interfaces 11 (2019) 39586–39593.
[83] E.A. Kwizera, W. Ou, S. Lee, et al., ACS Nano 16 (2022) 11374–11391.
[84] S. Wang, S. Hong, S. Cai, et al., J. Nanobiotechnol. 18 (2020) 70.
[85] L. Hui, Y. Su, T. Ye, et al., ACS Appl. Mater. Interfaces 10 (2018) 207–218.
[86] W. Jiang, L. Han, L. Yang, et al., Adv. Sci. 7 (2020) 2002259.
[87] S.B. Cheng, M.M. Chen, Y.K. Wang, et al., Anal. Chem. 93 (2021) 7102–7109.
[88] Y.K. Wang, M. Wang, S.B. Cheng, et al., View 4 (2023) 20220054.
[89] Y. Xiang, H. Zhang, H. Lu, et al., ACS Nano 17 (2023) 9633–9646.
[90] Z. Wang, X. Wan, S. Wang, Chem 9 (2023) 771–783.
[91] N. Sun, X. Li, Z. Wang, Y. Li, R. Pei, Biosens. Bioelectron. 102 (2018) 157–163.
[92] P.J. LeValley, M.W. Tibbitt, B. Noren, et al., Colloids Surf. B 174 (2019) 483–492.
[93] T. Li, N. Li, Y. Ma, et al., J. Mater. Chem. B 7 (2019) 6087–6098.
[94] P. Ding, Z. Wang, Z. Wu, et al., ACS Appl. Mater. Interfaces 12 (2020) 20263–20270.
[95] Y. Xiao, M. Wang, L. Lin, et al., Mater. Chem. Front. 2 (2018) 891–900.
[96] M. Wang, Y. Xiao, L. Lin, et al., Bioconjugate Chem. 29 (2018) 1081–1090.
[97] L. Chen, S. Huang, R.H. Ras, X. Tian, Nat. Rev. Chem. 7 (2023) 123–137.
[98] X. Zhou, Y. Zhang, K. Kang, et al., Anal. Chem. 94 (2022) 4650–4657.
[99] C. Shao, Y. Liu, J. Chi, et al., Research 2019 (2019) 9783793.
[100] X. Zhou, B. Luo, K. Kang, et al., Small 15 (2019) 1900558.
[101] J.N. Belling, L.K. Heidenreich, J.H. Park, et al., ACS Appl. Mater. Interfaces 12 (2020) 45744–45752.
[102] K. Xiong, W. Wei, Y. Jin, et al., Adv. Mater. 28 (2016) 7929–7935.
[103] Q. Meng, Y. Cheng, Q. Huang, et al., ACS Appl. Mater. Interfaces 11 (2019) 28732–28739.
[104] L. Rao, Q.F. Meng, Q. Huang, et al., Adv. Funct. Mater. 28 (2018) 1803531.
[105] F. Zhang, L. Wu, W. Nie, et al., Anal. Chem. 91 (2019) 15726–15731.
[106] G. Hvichia, Z. Parveen, C. Wagner, et al., Int. J. Cancer 138 (2016) 2894–2904.
[107] S. Wang, K. Liu, J. Liu, et al., Angew. Chem. 123 (2011) 3140–3144.
[108] H. Xu, B. Dong, S. Xu, et al., Biomaterials 138 (2017) 69–79.
[109] N. Sun, C. Zhang, J. Wang, et al., Nano Today 49 (2023) 12.
[110] Y. Xiao, M. Wang, L. Lin, et al., Nanomedicine 14 (2018) 183–199.
[111] J. Ling, D. Liu, J. Zhang, et al., ACS Nano 16 (2022) 20915–20921.